A peer-reviewed version of this preprint was published in PeerJ on 5 September 2017.

Haridas P, McGovern JA, McElwain SDL, Simpson MJ. 2017. Quantitative comparison of the spreading and invasion of radial growth phase and metastatic melanoma cells in a three-dimensional human skin equivalent model. PeerJ 5:e3754 https://doi.org/10.7717/peerj.3754

Quantitative comparison of the spreading and invasion of radial growth phase and metastatic melanoma cells in a three-dimensional human skin equivalent model

Parvathi Haridas[1,2], Jacqui A McGovern[1], D L Sean McElwain[1,2], Matthew J Simpson[1,2]

[1] Institute of Heath and Biomedical Innovation, Queensland University of Technology (QUT), Kelvin Grove 4059, Australia.

[2] School of Mathematical Sciences, QUT, PO Box 2434, Brisbane 4001, Australia.

Corresponding Author:

Matthew J Simpson[1,2]

QUT, PO Box 2434, Brisbane 4001, Australia

Email address: matthew.simpson@qut.edu.au

PeerJ Preprints | https://doi.org/10.7287/peerj.preprints.2984v1 | CC BY 4.0 Open Access | rec: 19 May 2017, publ: 19 May 2017

Abstract

Background: Standard two-dimensional (2D) cell migration assays do not provide information about vertical invasion processes, which are critical for melanoma progression. We provide information about three-dimensional (3D) melanoma cell migration, proliferation and invasion in a 3D melanoma skin equivalent (MSE) model. In particular, we pay careful attention to compare the structure of the tissues in the MSE with similarly-prepared 3D human skin equivalent (HSE) models. The HSE model is identically prepared to the MSE model except that melanoma cells are omitted. Using the MSE model, we examine melanoma migration, proliferation and invasion from two different human melanoma cell lines. One cell line, WM35, is associated with the early phase of the disease where spreading is thought to be confined to the epidermis. The other cell line, SK-MEL-28, is associated with the later phase of the disease where spreading into the dermis is expected.

Methods: 3D MSE and HSE models are constructed using human de-epidermised dermis (DED) prepared from skin tissue. Primary fibroblasts and primary keratinocytes are used in the MSE and HSE models to ensure the formation of a stratified epidermis, with a well-defined basement membrane. Radial spreading of cells across the surface of the HSE and MSE models is observed. Vertical invasion of melanoma cells downward through the skin layers is observed and measured using immunohistochemistry. All measurements of invasion are made at day 0, 9, 15 and 20, providing detailed time course data.

Results: Both HSE and MSE models are similar to native skin *in vivo*, with a well-defined stratification of the epidermis that is separated from the dermis by a basement membrane. In the HSE and MSE we find fibroblast cells confined to the dermis, and differentiated keratinocytes in the epidermis. In the MSE, melanoma cells form colonies in the epidermis during the early part of the experiment. In the later stage of the experiment, the melanoma cells in the MSE invade deeper into the tissues. Interestingly, both the WM35 and SK-MEL-28 melanoma cells lead to a breakdown of the basement membrane and eventually enter the dermis. However, these two cell lines invade at different rates, with the SK-MEL-28 melanoma cells invading faster than the WM35 cells.

Discussion: The MSE and HSE models are a reliable platform for studying melanoma invasion in a 3D tissue that is similar to native human skin. Interestingly, we find that the

PeerJ Preprints | https://doi.org/10.7287/peerj.preprints.2984v1 | CC BY 4.0 Open Access | rec: 19 May 2017, publ: 19 May 2017

WM35 cell line, that is thought to be associated with radial spreading only, is able to invade into the dermis. The vertical invasion of melanoma cells into the dermal region appears to be associated with a localised disruption of the basement membrane. Presenting our results in terms of time course data, along with images and quantitative measurements of the depth of invasion extends previous 3D work that has often been reported without these details.

PeerJ Preprints | https://doi.org/10.7287/peerj.preprints.2984v1 | CC BY 4.0 Open Access | rec: 19 May 2017, publ: 19 May 2017

1. Introduction

Melanoma is a deadly form of skin cancer (Bertolotto, 2013; Weinstein et al., 2014) that is caused by the malignant transformation of melanocytes in the skin, as illustrated in Fig. 1A (Uong & Zon, 2010; Bertolotto, 2013; Liu, Peng & Tobin, 2013). Even though melanoma is a rare form of skin cancer, melanoma accounts for 80% of skin cancer related deaths (Bandarchi et al., 2010; Bertolotto, 2013; Ramaraj & Cox, 2014; McCusker et al., 2017). The early stage of a primary melanoma, where cancer cells are confined to the epidermis, is known as the radial growth phase (RGP) (Meier et al., 2000). Melanoma in the RGP is curable through surgical removal (Weinstock, 2000; Cummins et al., 2006). However, survival rates of patients with melanoma at an advanced stage, where cancer cells have invaded vertically into the dermis, known as the vertical growth phase (VGP) and metastasised, is very low (Straume, Sviland & Akslen, 2000; Miller & Mihm, 2006; Sandru et al., 2014). The switch in progression, from radial spreading to vertical invasion is poorly understood (Hussein, 2004; Baruthio, Quadroni & Ruegg, 2008; Grahovac, Becker & Wells, 2013). Some cell lines are thought to be associated with the RGP (Bani et al., 1996; Cummins et al., 2006), whereas other cell lines are associated with more advanced stages of the disease (Fofaria & Srivastava, 2014; Tiwary et al., 2014). Thus, quantitative measurements of spreading and invasion of both RGP and metastatic cell lines in a three-dimensional (3D) human skin model could help improve our understanding of melanoma progression, and the characteristics of both radial and vertical spreading.

Previous studies about the spreading of melanoma have focused on examining the spatial extent population expansion, cell migration, cell proliferation, cell-to-cell adhesion and protein-expression on two-dimensional (2D) surfaces (Alexaki et al., 2010; Simpson et al., 2013; Treloar et al., 2014). These 2D studies are straightforward to perform and cost effective (Beaumont, Mohana-Kumaran & Haass, 2014; Johnston, Simpson & McElwain, 2014; Binny et al., 2016). Moreover, 2D models can be used for preliminary co-culture investigations to examine potential interactions between different cell types (Beaumont, Mohana-Kumaran & Haass, 2014; Haridas et al., 2017). This flexibility is very important for melanoma research. Co-culture assays are more realistic than monoculture assays since co-cultures allow melanoma cells to interact dynamically with other relevant cells, such as fibroblasts and keratinocytes (Gaggioli & Sahai, 2007; Li Fan & Houghton, 2007; Beaumont, Mohana-Kumaran & Haass, 2014; Sriram & Bigliardi-Qi, 2015).

PeerJ Preprints | https://doi.org/10.7287/peerj.preprints.2984v1 | CC BY 4.0 Open Access | rec: 19 May 2017, publ: 19 May 2017

Unfortunately, previous studies suggest that melanoma cells do not grow well in isolation (Beaumont, Mohana-Kumaran & Haass, 2014), and traditional 2D assays do not recreate a physiological environment similar to native human skin *in vivo*. Perhaps the most obvious limitation of 2D experiments is that they cannot be used to quantify vertical invasion (Van-Kilsdonk et al., 2010; Vorsmann et al., 2013; Kramer et al., 2013; Taloni et al., 2014). To improve our understanding of the differences between radial and vertical invasion, it is of interest to make time course observations and measurements of the spreading and invasion of melanoma in a 3D skin model (Brandner & Haass, 2013). Experimental studies focusing on melanoma spreading and invasion in 3D skin-based models have been described over the last 20 years. Table 1 compares key properties of some previous 3D skin-models using de-epidermised dermis (DED) to study melanoma progression and invasion. While other previous 3D models have been used, such as collagen-based models (Vorsmann et al., 2013), the brief review in Table 1 is restricted to those previous studies explicitly using 3D-DED models.

There has been extensive research focusing on 3D melanoma migration and spreading using cell lines that are associated with the metastatic phase of melanoma progression (Damsky, Rosenbaum & Bosenberg, 2010; Finn, Markovic & Joseph, 2012; Tiwary et al., 2014). However, in this work we are also interested in the switch from radial migration, confined to the epidermis and associated with the early phase of melanoma progression, to vertical invasion that is associated with more advanced melanoma progression. Therefore, we quantitatively compare the vertical invasive properties of two melanoma cell lines in a 3D skin model as a function of time. In particular, we compare results from one cell line that is associated with the early RGP stage of melanoma progression with results from another cell line that is linked with a more advanced, metastatic stage of the disease.

Previous studies demonstrate particular protocols of DED to construct human skin equivalent (HSE) models (Xie et al., 2010; Fernandez et al., 2014; McGovern et al., 2016). These 3D skin models are established *in vitro* and resemble native human skin *in vivo* as shown in Figs. 1B and 1C. One of our aims in this study is to adapt this skin model and introduce melanoma cells to establish a sustainable melanoma skin equivalent (MSE) model and recreate the different stages of melanoma progression. The other primary aim is to make quantitative

PeerJ Preprints | https://doi.org/10.7287/peerj.preprints.2984v1 | CC BY 4.0 Open Access | rec: 19 May 2017, publ: 19 May 2017

measurements of the depth of melanoma invasion as a function of time, and to use these measurements to examine differences between the two cell lines that we consider.

Two melanoma cell lines, WM35 (RGP) (Bani et al., 1996) and SK-MEL-28 (metastatic phase) (Fofaria & Srivastava, 2014) are grown in the MSE model over a period of 9, 15 and 20 days. We identify differences in behavior between the two cell lines, and in particular we quantify the vertical invasion of melanoma cells into the dermis over time. The conclusions facilitate an improved characterisation of MSE models, and the progression of RGP and metastatic phases of melanoma in realistic 3D environments, thereby extending previous 2D studies.

2. Experimental Methods

2.1 Keratinocyte isolation and culture

Queensland University of Technology (QUT) human research ethics provides written approval for the skin samples to be used in this study (approval number: QUT HREC #1300000063; UnitingCare Health 2003/46). The samples come from patients undergoing abdominoplasty surgery and breast reduction surgery (Xie et al., 2010).

Human keratinocyte cells are isolated from skin and cultured in full Green's medium following protocols described in Rheinwald & Green (1975), Dawson & Upton (2006) and by Haridas et al. (2016). Primary keratinocyte cells are cultured at 37 ^{o}C, in 5% CO_2 and 95% air.

2.2 Fibroblast isolation and culture

Human fibroblast cells are isolated following protocols in Haridas et al. (2017). Primary fibroblast cells are cultured at 37 ^{o}C, in 5% CO_2 and 95% air.

2.3 Melanoma cell culture

The human melanoma cell lines, WM35 and SK-MEL-28 are cultured as described in Haridas et al. (2016). WM35 melanoma cells are kindly donated by Professor Nikolas Haass

PeerJ Preprints | https://doi.org/10.7287/peerj.preprints.2984v1 | CC BY 4.0 Open Access | rec: 19 May 2017, publ: 19 May 2017

(University of Queensland Diamantina Institute) and SK-MEL-28 melanoma cells are donated by Professor Brian Gabrielli (Mater Research Institute-University of Queensland). Cells are cultured at 37 ^{o}C, in 5% CO_2 and 95% air.

2.4 Establishing HSE and MSE

HSE models are established using the skin collected from donors undergoing elective plastic surgery. The protocol for establishing the HSE model is given in Figs. 2A-2F. These protocols are adapted from previous work (Fernandez et al., 2014; McGovern et al., 2016). The DED is prepared following protocols described by Chakrabarty et al. (1999) and Dawson et al. (2006). In brief, to construct the HSE model, sterile stainless steel rings (Aix Scientifics, Germany) with a diameter of 6 mm are placed on the papillary side of the DEDs in a 24 well tissue culture plate (Nunc®, Australia). Primary keratinocyte cells ($2x10^4$) and primary fibroblast cells ($1x10^4$) are seeded onto the DEDs in full Green's medium and incubated at 37 ^{o} C, in 5% CO_2 and 95% air for 2 days. Subsequently, the DEDs with cells, from now onwards referred to as HSE, is submerged in full Green's medium for 2 days. These HSEs are then cultured at an air-liquid interface on sterile stainless steel grids with full Green's medium for 9, 15 and 20 days. HSE is also collected at day 0, just before the DED is lifted to the air-liquid interface, as a reference sample.

To construct the MSE models, we follow the same protocol for the HSE model, and include melanoma cells, WM35 ($5x10^3$) or SK-MEL-28 ($5x10^3$), in addition to primary keratinocyte ($2x10^4$) and primary fibroblast ($1x10^4$) cells on the individual DEDs. Experimental variability is assessed using triplicates for each cell line, and primary skin cells from three separate donors. This means that for each time point in our experiments we perform nine replicates, which accounts for biological and experimental variability. HSEs and MSEs are collected after day 0, 9, 15, and 20, and subjected to histological investigation.

2.5 MTT Assay

An MTT (3-(4,5-dimethylthiazol-2-yl)-2,5-diphenyltetrazolium bromide) (Thermo Scientific) assay is performed to check the viability of cells in the HSE and MSE models. HSE and MSEs collected on day 0, 9, 15 and 20 are submerged in 0.5 mg/ml w/v MTT solution and incubated at 37 ^{o} C, in 5% CO_2 and 95% air for 90 minutes. The metabolically active cells

PeerJ Preprints | https://doi.org/10.7287/peerj.preprints.2984v1 | CC BY 4.0 Open Access | rec: 19 May 2017, publ: 19 May 2017

cleave the tetrazolium salt into an insoluble purple formazan dye. The purple colour indicates metabolically active cells on the HSE and MSE models and these are imaged using a stereo microscope (Nikon SMZ 800) fitted with a Nikon digital camera.

2.6 Histological Analysis

Haemotoxylin and eosin (H&E) staining is used to characterise the tissue structure in the HSE and MSE models. MTT stained HSE and MSEs are fixed using 10% neutral buffered formalin (United Biosciences, Australia), processed in an automated vacuum tissue processor (Thermo Scientific, USA) and embedded in paraffin wax. All samples are sectioned to 5 µm thickness using a microtome (Leica RM2245, Leica Microsystems, Australia). Sections are first deparaffinised in 100% xylene and rehydrated in graded ethanol series of 100%, 90% and 70%, and followed by distilled water. These sections are incubated in Harris haematoxylin (HD Scientific, Australia) followed by differentiation with 1% acid alcohol, bluing with Scott's tap water solution and counterstaining with alcoholic eosin (HD Scientific). H&E stained sections are dehydrated in 90% and 100% ethanol, cleared with 100% xylene and mounted on coverslips using Pertex® mounting medium (Medite, Germany). All stained sections are imaged using an Olympus BX41 microscope fitted with an Olympus digital camera (Micropublisher, 3.3RTV, QImaging; Olympus, Q-Imaging, Tokyo, Japan).

2.7 Immunohistochemistry

Immunohistochemistry is performed on the paraffin-embedded (5 µm) sections. Paraffin embedded sections are deparaffinised and rehydrated as previously described in McGovern et al. (2013). HSE and MSE skin sections are subjected to heat-mediated antigen retrieval treatment using either sodium citrate buffer (pH 6.0) or EDTA buffer (pH 8.0) in a decloaking chamber (Biocare Medical, USA) as described in Table 2. All skin sections are washed in phosphate buffered saline followed by immunostaining using MACH 4™ Universal HRP polymer kit (Biocare Medical). The temperature and time varies for each marker, as outlined in Table 2. The primary antibody for each protein is diluted in DaVinci Green diluent (Biocare Medical) to concentrations specified in Table 2, and these sections are incubated with the primary antibody for the time specified in Table 2. All the sections are

PeerJ Preprints | https://doi.org/10.7287/peerj.preprints.2984v1 | CC BY 4.0 Open Access | rec: 19 May 2017, publ: 19 May 2017

finally counterstained using Gill's haematoxylin (HD Scientific), dehydrated, mounted and imaged as described in Section 2.6.

2.8 Image Analysis

We use ImageJ (Johnston, Simpson & McElwain, 2014; ImageJ, 2017) to measure the depth of melanoma cell invasion into the dermal region on the MSE models at different time points. The depth of melanoma invasion is taken to be the distance from the epidermal-dermal interface to the deepest region invaded by the melanoma cells, as shown in Figs. S1A-S1D.

3. Results and Discussion

3.1 Short tandem repeat profiling

Both melanoma cell lines, WM35 and SK-MEL-28, are validated using short tandem repeat profiling (Cell Bank, Australia. January 2015). This means that the cell lines that we use are identical to the reference samples held in Cell Bank.

3.2 MTT assay of HSE and MSE

We first outline the MTT assay performed on both the HSE and MSE models. Results of the MTT assay, shown in Fig. 3, reveal radial expansion of the populations of cells on the HSE and MSE models over time. The purple colour on these images shows viable cells migrating radially away from the central region where the cells were originally located at day 0, as in Figs. 3A, 3C and 3E. By day 9, the cells have migrated radially to reach to edge of the DED, as in Figs. 3B, 3D and 3F. This means that the population of cells in the HSE and MSE have spread radially, at least a distance of approximately 6 to 7 mm, over a period of 9 days as the purple colouration reaches the edge of the tissue. Consistent with this, we see that there are viable cells distributed right across the DED in both the HSE and MSE models after longer periods of time, shown in Fig. S2.

An interesting result detected by the MTT assay is the formation of visually prominent colonies of cells in the central region of the MSE for the SK-MEL-28 cell line at day 0 and day 9, as shown in the insets of Figs. 3E and 3F. Similarly, we also observe visually

PeerJ Preprints | https://doi.org/10.7287/peerj.preprints.2984v1 | CC BY 4.0 Open Access | rec: 19 May 2017, publ: 19 May 2017

prominent colonies of cells in the central region of the MSE for the WM35 cell line at day 0. Previous 3D skin models of melanoma progression also report the formation of visually-distinct colonies of cells on the surface of the DED, and these colonies are presumably made of melanoma cells (Dekker et al., 2000; Eves et al., 2000). Interestingly, we see that these distinct colonies of cells are no longer observed at day 15 or day 20 on the MSE with the SK-MEL-28 cell line, Fig. S2. Similarly, these distinct colonies of cells are no longer observed by day 9, 15 or 20 on the MSE with the WM35 cell line, Fig. 3D and Fig. S2. Since melanoma cells are thought to grow in colonies (Schwartz et al., 2008; Baraldi et al., 2013), a possible explanation for our observations is that the visually distinct dark purple colonies in the early period of the experiment could be groups of melanoma cells. As these colonies are not observed at later times, it is possible that these cells might have invaded deeper into the tissue, and are no longer present on the upper surface of the MSE. To confirm this conjecture, we now examine the distribution of different cell types within the HSE and MSE models. To do this we use histological analysis.

3.3 The HSE and MSE physiology resembles native human skin *in vivo*

The next aim in our study is to examine the tissue structure of the HSE and MSE models, and to compare the structure of the tissue in these models with the structure of native human skin *in vivo*. To investigate this, we perform histological analysis and describe our results in this section, Section 3.3. However, we also use immunohistochemistry to examine the spatial and temporal distribution of markers for cell migration, cell proliferation and cell invasion in Section 3.4. Since the main focus of this work is about cell migration, cell proliferation and cell invasion, we choose to present all histological analysis about tissue structure in the Supplemental Information document. However, we briefly describe the key points here.

Cross-sections through the HSE and MSE models are generated for H&E staining. Results at day 9, 15 and 20, showing HSE and MSE cross-sections, reveal morphological similarities to native human skin *in vivo.* In particular, we see the formation of distinct epidermal and dermal regions, Figs. S3B-S3D, Figs. S4B-S4D and Figs. S5B-S5D. These images show that keratinocytes stratify into well-defined layers: stratum basale; stratum granulosum; stratum spinosum; and stratum corneum, which are a characteristic of native human skin (Wikramanayake, Stojadinovic & Tomic-Canic, 2014) as shown in Figs. 1B and 1C, Figs. S3A-S3D, Figs. S4A-S4D and Figs. S5A-S5D. However, H&E staining in Fig. S3A, Fig.

PeerJ Preprints | https://doi.org/10.7287/peerj.preprints.2984v1 | CC BY 4.0 Open Access | rec: 19 May 2017, publ: 19 May 2017

S4A and Fig. S5A, of HSE and MSE cross-sections at day 0, are consistent with the early stages of epidermal and dermal formation, which then matures with time. In summary, we observe mature stratification after 9 days, and this is consistent with previous investigations (Topping et al., 2008).

The basement membrane separates the epidermal and dermal layers, and is a prominent feature of native human skin *in vivo* (Marinkovich et al., 1993; Golan et al., 2015). The basement membrane is particularly important in the context of melanoma progression because melanoma confined to the epidermal layer can be successfully treated by surgical removal, whereas the prognosis for melanoma that has spread into the dermis is poor (Weinstock, 2000; Cummins et al., 2006; Bertolotto, 2013; Sandru et al., 2014). The positive immunohistological staining is obtained using the marker collagen IV (Col IV). Immunohistological examinations of the HSE and MSE cross-sections show positive staining of the basement membrane at day 9, 15 and 20, as shown in Figs. S3F-S3H, Figs. S4F-S4H and Figs. S5F-S5H. However, all cross-sections of the skin models at day 0 show minimal positive staining. This is consistent with the initial development of the basement membrane, as highlighted by the arrows in Fig. S3E, Fig. S4E and Fig. S5E. Conversely, only intermittent Col IV staining is present in the MSE models at day 9, 15 and 20, as shown in Figs. S4F-S4H and Figs. S5F-S5H. We hypothesise that these results could be caused by melanoma cells disrupting the basement membrane and invading into the dermal region. Metastatic melanoma cells in particular are associated with dermal invasion *in vivo* by disturbing the basement membrane (Golan et al., 2015; Sandri et al., 2016). Therefore, this result further suggests that the MSE models recapitulates certain *in vivo* stages of melanoma progression *in vitro*.

Lastly, positive staining of the terminally differentiating epidermis confirms that both the HSE and MSE models constructed *in vitro* are similar to native human skin *in vivo*. The marker loricrin identifies terminally differentiating cells in the epidermis (Nithya, Radhika & Jeddy, 2015). Therefore, loricrin staining of HSE and MSE cross-sections, as shown in Figs. S3J-S3L, Figs. S4J-S4L and Figs. S5J-S5L, at day 9, 15 and 20, suggest that the epidermal structure in the HSE and MSE models is consistent with native human skin. However, results at day 0 from cross-sections of HSE and MSE models, shown in Fig. S3I, Fig. S4I and Fig. S5I, do not have any positive loricrin staining. Loricrin is known to be absent on non-stratified epithelium (Nithya, Radhika & Jeddy, 2015). Hence, the negative result at day 0 is

PeerJ Preprints | https://doi.org/10.7287/peerj.preprints.2984v1 | CC BY 4.0 Open Access | rec: 19 May 2017, publ: 19 May 2017

probably due to the absence of the stratum corneum on day 0, which is consistent with an immature epidermis.

In summary, the loricrin staining suggests that the physiology of the HSE and MSE models is consistent with native skin. Furthermore, our findings show that HSE models have well-defined stratified epidermal and dermal regions that are separated by a basement membrane. This confirms that the *in vitro* HSE model is consistent with native human skin *in vivo*. In contrast, the MSE models do not always have a well-defined basement membrane. At early times in the experiments we see that the basement membrane is formed and present in the MSE model. However, at later times, the basement membrane in the MSE model is partially absent. These differences between the MSE and HSE models suggest that the presence of melanoma cells in the MSE models might lead to disruptions in the basement membrane. Furthermore, we hypothesise that this disruption is associated with vertical invasion.

3.4 Proliferation, migration and invasion of melanoma cells on the MSE model

Certain key features of cancer progression, including melanoma, are thought to be the proliferation, migration and invasion of cancer cells (Hanahan & Weinberg, 2000). Therefore, we aim to explore the spatial and temporal distributions of these features in the HSE and MSE models. In particular, we use specific markers for cell migration, cell proliferation and cell invasion in our 3D models.

The MTT assay provides information about the radial spreading of cells across the MSE model. In addition to radial spreading, we also aim to observe and quantify the vertical invasion of melanoma cells, and in particular we wish to focus on cell lines that are associated with both the early and later stages of melanoma progression. To make this comparison we examine data from the MSE with the WM35 melanoma cell line in Fig. 4, with results using the SK-MEL-28 cell line in Fig. 5. Immunohistochemistry results in Fig. 4 and Fig. 5 indicate the migration, proliferation and invasion patterns of WM35 and SK-MEL-28 cell lines, respectively. We first identify actively proliferating cells in the MSE using the Ki-67 marker. Results in Figs. 4A-4D and Figs. 5A-5D highlight positively stained cells at day 0, 9, 15 and 20 for the WM35 and SK-MEL-28 cell lines, respectively. It is important to note that the Ki-67 marker identifies all proliferating cells, and does not distinguish between proliferating fibroblast cells, proliferating keratinocyte cells and proliferating melanoma

PeerJ Preprints | https://doi.org/10.7287/peerj.preprints.2984v1 | CC BY 4.0 Open Access | rec: 19 May 2017, publ: 19 May 2017

cells. Therefore, additional information is required to distinguish between these different types of cells. Overall, we see that there are proliferative cells in both the epidermal and dermal regions of the tissue.

Migrating cells in the MSE models are detected using the marker vimentin (Chernoivanenko, Minin &Minin, 2013). It is challenging to identify the particular type of migrating cells using vimentin, as vimentin is expressed by most mesenchymal cell types (Goodpaster et al., 2008; Chernoivanenko, Minin &Minin, 2013). Since both fibroblasts and melanoma cell lines are mesenchymal (Goodpaster et al., 2008; Kim et al., 2013; Sriram & Bigliardi-Qi, 2015) we expect that all melanoma and fibroblast cells will be positive for vimentin. To potentially distinguish between melanoma cells and fibroblast cells in the MSE models, we note that fibroblasts can be identified since they tend to be isolated and they have an elongated cellular morphology (Sriram & Bigliardi-Qi, 2015). Furthermore, some of the vimentin positive cells appear to be arranged in colonies, and this is consistent with typical melanoma morphology (Schwartz et al., 2008; Kim et al., 2010; Baraldi et al., 2013). With this additional information, vimentin can be used to indicate the spatial distribution of fibroblasts, which appear to be only present in the dermal region, as shown in Figs. 4E-4H in the MSE with the WM35 melanoma cell line, and in Figs. 5E-5H in the MSE with the SK-MEL-28 melanoma cell line, at day 0, 9, 15 and 20. The fact that we tend to see fibroblast cells in the dermal region only provides further evidence that the MSE models resemble the HSE model, as shown in Fig. 6, as well as native human skin *in vivo* (Sriram & Bigliardi-Qi, 2015). Since fibroblast cells have migrated vertically downward, into the dermis, our MSE and HSE models also capture a key feature of native human skin, as fibroblasts are typically confined to the dermal region (Driskell & Watt, 2015). Vimentin positive melanoma cells, arranged in colonies, are detected in both the epidermal and dermal region of the MSE models, as shown in Figs. 4E-4H and Figs. 5E-5H, at day 0, 9, 15 and 20. All of the interpretations of the type of vimentin positive cells involve some subjective assessment of whether the cells are elongated or whether they appear to be arranged in colonies. To provide further information to distinguish between melanoma cells and fibroblast cells, we now use a specific marker for melanoma cells (Haridas et al., 2016).

Vertical invasion of melanoma cells into the MSEs is detected by the marker S100. Our previous studies show that S100 is a reliable marker that identifies both the WM35 and the SK-MEL-28 melanoma cell lines (Haridas et al., 2016; Haridas et al., 2017). In both MSE

PeerJ Preprints | https://doi.org/10.7287/peerj.preprints.2984v1 | CC BY 4.0 Open Access | rec: 19 May 2017, publ: 19 May 2017

models with the WM35 cell line and the SK-MEL-28 cell line, colonies of melanoma cells are present at day 0, 9, 15 and 20. Individual cells within these colonies are positively stained by S100. Smaller colonies of melanoma cells are initially present near the upper surface of the MSE models, as shown in Fig. 4I and Fig. 5I. These melanoma colonies dramatically increase in size and number with time, and the melanoma colonies invade into the dermis after day 15 and 20, as shown in Figs. 4K and 4L for the WM35 melanoma cell line, and after day 9 in Figs. 5J-5L for the SK-MEL-28 melanoma cell line. Comparing the size of the melanoma colonies over time in both MSE models shows that the colonies of SK-MEL-28 melanoma cells are larger than the colonies of WM35 melanoma cells. These differences are most evident at day 20, as shown by comparing the images in Fig. 4L and Fig. 5L. These results suggest that the SK-MEL-28 cell line is more aggressive than the WM35 melanoma cell line. This difference is consistent with the usual notion that the SK-MEL-28 melanoma cell line is associated with the later, more aggressive stage of the disease, whereas the WM35 melanoma cell line is associated with the early phase of melanoma progression. Also, it is possible that these immunohistochemistry results are consistent with the previous MTT results in Figs. 3E and 3F since the colonies of cells on the surface of the DED seem to disappear at later times. This could be a result of the melanoma cells invading deeper into the MSE tissue at later times and therefore disappearing from the surface of the DED, as shown in Fig. S2.

An interesting result from the MSE with the WM35 melanoma cell line is that we observe the invasion of small colonies of WM35 melanoma cells into the dermis at day 20, as shown in Fig. 4L. This result is interesting because WM35 melanoma cells are thought to be associated with the early phase of melanoma progression, where cells are believed to be limited to the epidermis (Gaggioli & Sahai, 2007). Previous 3D studies suggest that cells from the early RGP are restricted in the epidermal region only (Dekker et al., 2000; Beaumont, Mohana-Kumaran & Haass, 2014). Therefore, our results are contradictory, suggesting that WM35 cells are able to breach the basement membrane and invade into the dermis in our MSE model.

Overall, these results showcase the successful establishment of a reliable and enduring MSE model that can be used to examine the migration, proliferation and invasion of melanoma cells from different cell lines associated with different stages of melanoma progression. However, in addition to providing qualitative information about the spatial and temporal

PeerJ Preprints | https://doi.org/10.7287/peerj.preprints.2984v1 | CC BY 4.0 Open Access | rec: 19 May 2017, publ: 19 May 2017

distribution of different cell types in the MSE models, we also provide quantitative information about the invasion process.

3.5 Quantification of melanoma invasion

To further examine the differences in the invasion patterns associated with the WM35 and SK-MEL-28 melanoma cell lines, we measure the depth of cell invasion into the dermal region over time. The depth of invasion is taken to be the distance between the epidermal-dermal interface to the deepest region invaded by the melanoma cells, as shown in Figs. S1A-S1C. The invasion depth is measured in each experiment, at each time point, using ImageJ (ImageJ, 2017). Each measurement is repeated using three biological replicates, and the average depth is calculated by averaging the data across the three biological replicates.

Results in Fig. 7 show that the SK-MEL-28 melanoma cells invade earlier, deeper and faster than the WM35 melanoma cells. For example, at day 0 neither the SK-MEL-28 nor the WM35 melanoma cells appear to be in the dermis, even with minimal basement membrane present. However, by day 9, the SK-MEL-28 melanoma cells have invaded into the dermis, whereas the WM35 melanoma cells are still contained within the epidermis.

Previous research has measured the invasion of melanoma cells into the dermis (Eves et al., 2003a; Eves et al., 2003b; Marques and Mac Neil, 2016). These studies use a semi-quantitative measurement of cell counts, showing various metastatic melanoma cells invading the dermal region. It is interesting to note that our study of melanoma invasion using MSE models differs from previous approaches, as shown in Table 1. We use a simple method of visual analysis and measurement of melanoma cell invasion into the dermal region. Most importantly, we provide time course measurements of melanoma cell invasion.

In summary our results suggest that the WM35 and the SK-MEL-28 melanoma cell lines both exhibit invasive properties. This is interesting because the WM35 melanoma cell line is thought to be associated with the early phase of melanoma progression where the cells are confined to the epidermis. However, our qualitative observations and quantitative measurements suggest that the WM35 melanoma cell line is less invasive than the SK-MEL-28 melanoma cell line. Overall, these qualitative and quantitative comparisons suggest that the MSE model described here can be used as a reliable platform to study both the early and

PeerJ Preprints | https://doi.org/10.7287/peerj.preprints.2984v1 | CC BY 4.0 Open Access | rec: 19 May 2017, publ: 19 May 2017

later stages of melanoma progression simply by using cells from different melanoma cell lines in the same MSE.

4. Conclusion

In summary, 3D skin model studies are more realistic, and more closely resemble native human skin *in vivo* than 2D studies. HSE skin models constructed using DED are used in many research areas including wound healing and burn studies (Topping et al., 2006; Xie et al., 2010; Monsuur et al., 2016). Since the physiological architecture of the HSE model is similar to native human skin *in vivo* it can be adapted to study melanoma proliferation, migration and invasion patterns. Melanoma has various phases of progression and 2D models are limited since 2D models cannot be used to study vertical invasion. In contrast, 3D skin-based melanoma models can be used to study vertical invasion, as well as exploring how melanoma cells interact with surrounding cells and tissues.

In this study we develop an *in vitro* MSE model using cell lines from early and late phases of melanoma. The MSE model incorporates ether WM35 melanoma cells or SK-MEL-28 melanoma cells, as well as primary keratinocytes and primary fibroblasts. Our MSE models are capable of examining melanoma progression for up to 20 days, which is the longest time point we have analysed. Collectively, our results suggest that MSE models constructed *in vitro* have similar tissue structure to native human skin. The melanoma cells in the MSE models proliferate, migrate and invade into the dermis as observed in native human skin *in vivo*. However, melanoma cells lines from different phases of the disease lead to different patterns of invasion. Importantly, the MSE models enable quantitative measurements of the invasive process to be made, and allow us to quantitatively compare the progression of the two different cell lines.

Acknowledgements

We thank Professor Nikolas Haass and Professor Brian Gabrielli for providing the melanoma cell lines, WM35 and SK-MEL-28.

Author contributions

Parvathi Haridas: Conceived and designed the experiments, performed the experiments, analysed the data, wrote the paper, prepared figures and tables, and reviewed drafts of the paper.

Jacqui McGovern: Conceived and designed the experiments, helped analyse the data, and reviewed drafts of the paper.

DL Sean McElwain: Conceived and designed the experiments, helped analyse the data, and reviewed drafts of the paper

Matthew Simpson: Conceived and designed the experiments, helped analyse the data, and reviewed drafts of the paper.

Funding

We acknowledge funding from the Australian Research Council (DP170100474).

References

1. Alexaki VI, Javelaud D, Van-Kempen LCL, Mohammed KS, Dennler S, Luciani F, Hoek KS, Juarez P, Goydos JS, Fournier PJ, Sibon C, Bertolotto C, Verrecchia F, Saule S, Delmas V, Ballotti R, Larue L, Saiag P, Guise TA, Mauviel A. 2010. GL12-mediated melanoma invasion and metastasis. *Journal of the National Cancer Institute* 102:1148-1159.
2. Bandarchi B, Ma L, Navab R, Seth A, Rasty G. 2010. From melanocyte to malignant metastatic melanoma. *Dermatology Research and Practice* 2010:583748.
3. Bani MR, Rak J, Adachi D, Wiltshire R, Trent JM, Kerbel RS, Ben-David Y. 1996. Multiple features of advanced melanoma recapitulated in tumorigenic variants of early stage (radial growth phase) human melanoma cell lines: evidence for a dominant phenotype. *Cancer Research* 56:3075-3086.
4. Baraldi MM, Alemi AA, Sethna JP, Caracciolo S, Porta CALM, Zapperi S. 2013. Growth and form of melanoma colonies. *Journal of Statistical Mechanics-Theory and Experiment* 2013:p02032.
5. Baruthio F, Quadroni M, Ruegg C, Mariotti A. 2008. Proteomic analysis of membrane rafts of melanoma cells identifies protein patterns characteristic of the tumor progression stage. *Proteomics* 8:4733-4747.
6. Beaumont KA, Mohana-Kumaran N, Haass NK. 2014. Modelling melanoma *in vitro* and *in vivo*. *Healthcare* 2:27-46.
7. Bechetoille N, Haftek M, Staquet MJ, Cochran AJ, Schmitt D, Berthier-Vergnes O. 2000. Penetration of human metastatic melanoma cells through an authentic dermal-epidermal junction is associated with dissolution of native collagen IV and VII. *Melanoma Research* 10:427-434.
8. Bertolotto C. 2013. Melanoma: from melanocyte to genetic alterations and clinical options. *Scientifica* 2013:635203.
9. Binny RN, Haridas P, James A, Law R, Simpson MJ, Plank MJ. 2016. Spatial structure arising from neighbour-dependent bias in collective cell movement. *PeerJ* 4:e1689.
10. Brandner JM, Haass NK. 2013. Melanoma's connections to the tumour microenvironment. *Pathology* 45:443-452.
11. Chakrabarty KH, Dawson RA, Harris P, Layton C, Babu M, Gould L, Phillips J, Leigh I, Green C, Freedlander E, Mac Neil S. 1999. Development of autologous

PeerJ Preprints | https://doi.org/10.7287/peerj.preprints.2984v1 | CC BY 4.0 Open Access | rec: 19 May 2017, publ: 19 May 2017

human dermal-epidermal composites based on sterilized human allodermis for clinical use. *British Journal of Dermatology* 141:811-823.

12. Chernoivanenko IS, Minin AA, Minin AA. 2013. Role of vimentin in cell migration. *Russian Journal of Developmental Biology* 44:186-202.
13. Cummins DL, Cummins JM, Pantle H, Silverman MA, Leonard AL, Chanmugam A. 2006. Cutaneous malignant melanoma. *Mayo Clinic Proceedings* 81:500-507.
14. Damsky WE, Rosenbaum LE, Bosenberg M. 2010. Decoding melanoma metastasis. *Cancers* 3:126-163.
15. Dawson RA, Upton Z, Malda J, Harkin DG. 2006. Preparation of cultured skin for transplantation using insulin-like growth factor I in conjunction with insulin-like growth factor binding protein 5, epidermal growth factor, and vitronectin. *Tranplantation* 81:1668-1676.
16. Dekker SK, Van-Doorn R, Kempenaar J, Gruis NA, Vermeer BJ, Ponec M. 2000. Skin equivalent: an attractive model to evaluate early melanoma metastasis. *Melanoma Research* 10:127-140.
17. Dennhofer R, Kurschat P, Zirgrino P, Klose A, Bosserfoff A, Van-Muijen G, Krieg T, Mauch C, Hunzelmann N. 2003. Invasion of melanoma cells into the dermal connective tissue in vitro: evidence for an important role of cysteine proteases. *International Journal of Cancer* 106:316-323.
18. Driskell RR, Watt FM. 2015. Understanding fibroblast heterogeneity in the skin. *Trends in Cell Biology* 25:92-99.
19. Eves P, Layton C, Hedley S, Dawson RA, Wagner M, Morandini R, Ghanem G, Mac Neil S. 2000. Characterization of an *in vitro* model of human melanoma invasion based on reconstructed human skin. *British Journal of Dermatology* 142:210-222.
20. Eves P, Katerinaki E, Simpson C, Layton C, Dawson R, Evans G, Mac Neil S. 2003a. Melanoma invasion in reconstructed human skin is influenced by skin cells – investigation of the role of proteolytic enzymes. *Clinical and Experimental Metastasis* 20:685-700.
21. Eves P, Haycock J, Layton C, Wagner M, Kemp H, Szabo M, Morandini R, Ghanem G, Garcia-Borron JC, Jimenez-Cervantes C, Mac Neil S. 2003b. Anti-inflammatory and anti-invasive effects of α-melanocyte-stimulating hormone in human melanoma cells. *British Journal of Cancer* 89:2004-2015.

22. Fernandez TL, Lonkhuyzen DRV, Dawson RA, Kimlin MG, Upton Z. 2014. Characterization of a human skin equivalent model to study the effects of ultraviolet B radiation on keratinocytes. *Tissue Engineering Part C Methods* 20:588-598.
23. Finn L, Markovic SN, Joseph RW. 2012. Therapy for metastatic melanoma: the past, present, and future. *BMC Medicine* 10:23.
24. Fofaria N, Srivastava SK. 2014. Critical role of STAT3 in melanoma metastasis through anoikis resistance. *Oncotarget* 5:7051-7064.
25. Gaggioli C, Sahai E. 2007. Melanoma invasion – current knowledge and future directions. *Pigment Cell and Melanoma Research* 20:161-172.
26. Golan T, Messer AR, Amitai-Lange A, Melamed Z, Ohana R, Bell RE, Kapitansky O, Lerman G, Greenberger S, Khaled M, Amar N, Albrengues J, Gaggioli C, Gonen P, Tabach Y, Sprinzak D, Shalom-Feuerstein R, Levy C. 2015. Interactions of melanoma cells with distal keratinocytes trigger metastasis via Notch signaling of inhibition of MITF. *Molecular Cell* 59:664-676.
27. Goodpaster T, Legesse-Miller A, Hameed MR, Aisner SC, Randolph-Habecker J, Coller HA. 2008. An immunohistochemical method for identifying fibroblasts in formalin-fixed, paraffin-embedded tissue. *Journal of Histochemistry and Cytochemistry* 56:347-358.
28. Grahovac J, Becker D, Wells A. 2013. Melanoma cell invasiveness is promoted at least in part by the Epidermal Growth Factor-like repeats of Tenascin-C. *The Journal of Investigative Dermatology* 133:210-220.
29. Hanahan D, Weinberg RA. 2000. The hallmarks of cancer. *Cell* 100:57-70.
30. Haridas P, McGovern JA, Kashyap AS, McElwain DLS, Simpson MJ. 2016. Standard melanoma-associated markers do not identify the MM127 metastatic melanoma cell line. *Scientific Reports* 6:24569.
31. Haridas P, Penington CJ, McGovern JA, McElwain DLS, Simpson MJ. 2017. Quantifying rates of cell migration and cell proliferation in co-culture barrier assays reveals how skin and melanoma cells interact during melanoma spreading and invasion. *Journal of Theoretical Biology* 423:13-25.
32. Hussein MR. 2004. Genetic pathways to melanoma tumorigenesis. *Journal of Clinical Pathology* 57:797-801.
33. ImageJ, ImageJ User Guide: Research Services Branch, National Institute of Health. https://imagej.nih.gov/ij/docs/guide/146-29.html (accessed May 2017).

640 34. Johnston ST, Simpson MJ, McElwain DLS. 2014. How much information can be
641 obtained from tracking the position of the leading edge in a scratch assay? *Journal of*
642 *the Royal Society Interface* 11:20140325.
643 35. Kim TK, Chen J, Li W, Zjawiony J, Miller D, Janjetovic Z, Tuckey RC, Slominski A.
644 2010. A new steroidal 5,7-diene derivative, 3β-hydroxyandrosta-5,7-diene-17β-
645 carboxylic acid, shows potent anti-proliferative activity. *Steroids* 75:230-239.
646 36. Kim JE, Leung E, Baguley BC, Finlay GJ. 2013. Heterogeneity of expression of
647 epithelial-mesenchymal transition markers in melanocytes and melanoma cell lines.
648 *Frontiers in Genetics* 4:e97.
649 37. Kramer N, Walzl A, Unger C, Rosner M, Krupitza G, Hengstschlager M, Dolznig H.
650 2013. In vitro cell migration and invasion assays. *Mutation Research* 752:10-24.
651 38. Li H, Fan X, Houghton J. 2007. Tumor microenvironment: the role of the tumor
652 stroma in cancer. *Journal of Cellular Biochemistry* 101:805-815.
653 39. Liu W, Peng Y, Tobin DJ. 2013. A new 12-gene diagnostic biomarker signature of
654 melanoma revealed by integrated microarray analysis. *PeerJ* 1:e49.
655 40. Mac Neil S, Eves P, Richardson B, Molife R, Lorigan P, Wagner M, Layton C,
656 Morandini R, Ghanem G. 2000. Oestrogenic steroids and melanoma cell interaction
657 with adjacent skin cells influence invasion of melanoma cells in vitro. *Pigment Cell*
658 *and Melanoma Research* 13:68-72.
659 41. Marck VV, Stove C, Bossche KVD, Stove V, Paredes J, Haeghen YV, Bracke M.
660 2005. P-cadherin promotes cell-cell adhesion and counteracts invasion in human
661 melanoma. *Cancer Research* 65:8774-8783.
662 42. Marinkovich MP, Keene DR, Rimberg CS, Burgeson RE. 1993. Cellular origin of the
663 dermal-epidermal basement membrane. *Developmental Dynamics* 197:255-267.
664 43. Marques CMdG, Mac Neil S. 2016. Use of a tissue engineered human skin model to
665 investigate the effects of wounding and of an anti-inflammatory on melanoma cell
666 invasion. *PLoS ONE* 11:e0156931.
667 44. Meier F, Nesbit M, Hsu M, Martin B, Belle P, Elder DE, Schaumburg-Lever G,
668 Garbe C, Walz TM, Donatien P. 2000. Human melanoma progression in skin
669 reconstructs: biological significance of bFGF. *The American Journal of Pathology*
670 156:193-200.
671 45. McGovern JA, Heinemann JR, Burke LJ, Dawson R, Parker TJ, Upton Z, Hooper JD,
672 Manton KJ. 2013. Stratum basale keratinocyte expression of the cell-surface

glycoprotein CDCP1 during epidermogenesis and its role in keratinocyte migration. *British Journal of Dermatology* 168:496-503.

46. McGovern JA, Meinert C, de Veer SJ, Hollier BG, Parker TJ, Upton Z. Attenuated kallikrein-related peptidase activity disrupts desquamation and leads to stratum corneum thickening in human skin equivalent models. *British Journal of Dermatology* 176:145-158.
47. McCusker JP, Dumontier M, Yan R, He S, Dordick JS, McGuinness DL. 2017. Finding melanoma drugs through a probabilistic knowledge gap. *PeerJ* 3:e106.
48. Miller AJ, Mihm MC. 2006. Melanoma. *The New England Journal of Medicine* 355:51-65.
49. Monsuur HN, Boink MA, Weijers EM, Roffel S, Breetveld M, Gefen A, van den Broek LJ, Gibbs S. 2016. Methods to study cell mobility during skin wound healing *in vitro*. *Journal of Biomechanics* 49:1381-1387.
50. Nithya S, Radhika T, Jeddy N. 2015. Loricrin- an overview. *Journal of Oral and Maxillofacial Pathology* 19:64-68.
51. Peinado H, Aleckovic M, Lavotshkin S, Matei I, Costa-Silva B, Moreno-Bueno G, Hergueta-Redondo M, Williams C, Garcia-Santos G, Ghajar CM, Niadori-Hoshino A, Hoffman C, Bdal K, Garcia BA, Callahan MK, Yuan J, Martins VR, Skog J, Kaplan RN, Brady MS, Wolchok JD, Chapman PB, Kang Y, Bromberg J, Lyden D. 2012. Melanoma exosomes educate bone marrow progenitor cells toward a pro-metastatic phenotype through MET. *Nature Medicine* 18:883-891.
52. Pope JH, Morrison L, Moss DJ, Parsons PG, Regius MS. 1979. Human malignant melanoma cell lines. *Pathology* 11:191-195.
53. Ramaraj P, Cox JL. 2014. In-vitro effects of sex steroids on mouse melanoma (B16F10) cell growth. *CellBio* 3:60-71.
54. Rheinwald JG, Green H. 1975. Serial cultivation of strains of human epidermal keratinocytes: the formation of keratinizing colonies from single cells. *Cell* 6:331-343.
55. Sandri S, Faiao-Flores F, Tiago M, Pennacchi PC, Massaro RR, Alves-Fernandes DK, Berardinelli GN, Evangelista AF, Vazquez VL, Reis RM, Maria-Engler SS. 2016. Vemurafenib resistance increases melanoma invasiveness and modulates the tumor microenvironment by MMP-2 upregulation. *Pharmacological Research* 111:523-533.
56. Sandru V, Voinea S, Panaitescu E, Blidaru A. 2014. Survival rates of patients with metastatic malignant melanoma. *Journal of Medicine and Life* 7:572-576.

57. Simpson MJ, Treloar KK, Binder BJ, Haridas P, Manton KJ, Leavesley DI, McElwain DLS, Baker RE. 2013. Quantifying the roles of ell motility and cell proliferation in a circular barrier assay. *Journal of the Royal Society Interface* 10:20130007.
58. Schwartz MA, McRoberts K, Coyner M, Andarawewa KL, Frierson HFJr, Sanders JM, Swenson S, Markland F, Conaway MR, Theodorescu D. 2008. Integrin agonists as adjuvants in chemotherapy for melanoma. *Clinical Cancer Research* 14:6193-6197.
59. Sriram G, Bigliardi-Qi M. 2015. Fibroblast heterogeneity and its implications for engineering organotypic skin models in vitro. *European Journal of Cell Biology* 94:483512.
60. Straume O, Sviland L, Akslen LA. 2000. Loss of nuclear p16 protein expression correlates with increased tumor cell proliferation (Ki-67) and poor prognosis in patients with vertical growth phase. *Clinical Cancer Research* 6:1845-1853.
61. Taloni A, Alemi AA, Ciusani E, Sethna JP, Zapperi S, La-Porta CA. 2014. Mechanical properties of growing melanocyte nevi and the progression to melanoma. *PLoS One* 9:e94229.
62. Tiwary S, Preziosi M, Rothberg PG, Zeitouni N, Corson N, Xu L. 2014. ERBB3 is required for metastasis formation of melanoma cells. *Oncogenesis* 3:e110.
63. Topping G, Malda J, Dawson RA, Upton Z. 2006. Development and characterisation of human skin equivalents and their potential application as a burn wound model. *Primary Intention* 14:14-21.
64. Treloar KK, Simpson MJ, Haridas P, Manton KJ, Leavesley DI, McElwain DLS, Baker RE. 2013. Multiple types of data are required to identify the mechanisms influencing the spatial expansion of melanoma cell colonies. *BMC Systems Biology* 7:137.
65. Treloar KK, Simpson MJ, Binder BJ, McElwain DLS, Baker RE. 2014. Assessing the role of spatial correlations during collective cell spreading. *Scientific Reports* 4:5713.
66. Uong A, Zon LI. 2010. Melanocytes in development and cancer. *Journal of Cellular Physiology* 222:38-41.
67. Van-Kilsdonk JWJ, Wilting RH, Bergers M, van Muijen GNP, Schalkwijk J, van Kempen LCLT, Swart GWM. 2008. Attenuation of melanoma invasion by a secreted variant of activated leukocyte cell adhesion molecule. *Cancer Research* 68:3671-3679.

68. Van-Kilsdonk JW, Bergers M, Van Kempen LC, Schalkwijk J, Swart GW. 2010. Keratinocytes drive melanoma invasion in a reconstructed skin model. *Melanoma Research* 20:372-380.
69. Vorsmann H, Groeber F, Walles H, Busch S, Beissert S, Walczak H, Kumls D. 2013. Development of a human three-dimensional organotypic skin-melanoma spheroid model for *in vitro* drug testing. *Cell Death and Disease* 4:e719.
70. Weinstein D, Leininger J, Hamby C, Safai B. 2014. Diagnostic and prognostic biomarkers in melanoma. *The Journal of Clinical and Aesthetic Dermatology* 7:13-24.
71. Weinstock MA. 2000. Early detection of melanoma *JAMA-Journal of the American Medical Association* 284:886-889.
72. Wikramanayake TC, Stojadinovic O, Tomic-Canic M. 2014. Epidermal differentiation in barrier maintenance and wound healing. *Advances in Wound Care* 3:272-280.
73. Xie Y, Rizzi SC, Dawson RA, Lynam E, Richards S, Leavesley DI, Upton Z. 2010. Development of a three-dimensional human skin equivalent wound model for investigating novel wound healing therapies. *Tissue Engineering Part C-Methods* 16:1111-1123.
74. Yang Y, Sule-Suso J, Sockalingum GD. 2008. Study of melanoma invasion by FTIR spectroscopy. *Progress in Biomedical Optics and Imaging- Proceedings of SPIE* 6859:68591U
75. Zaidi MR, Day C, Merlino G. 2008. From UV's to metastases: modelling melanoma initiation and progression in the mouse. *Journal of Investigative Dermatology* 128:2381-2391.

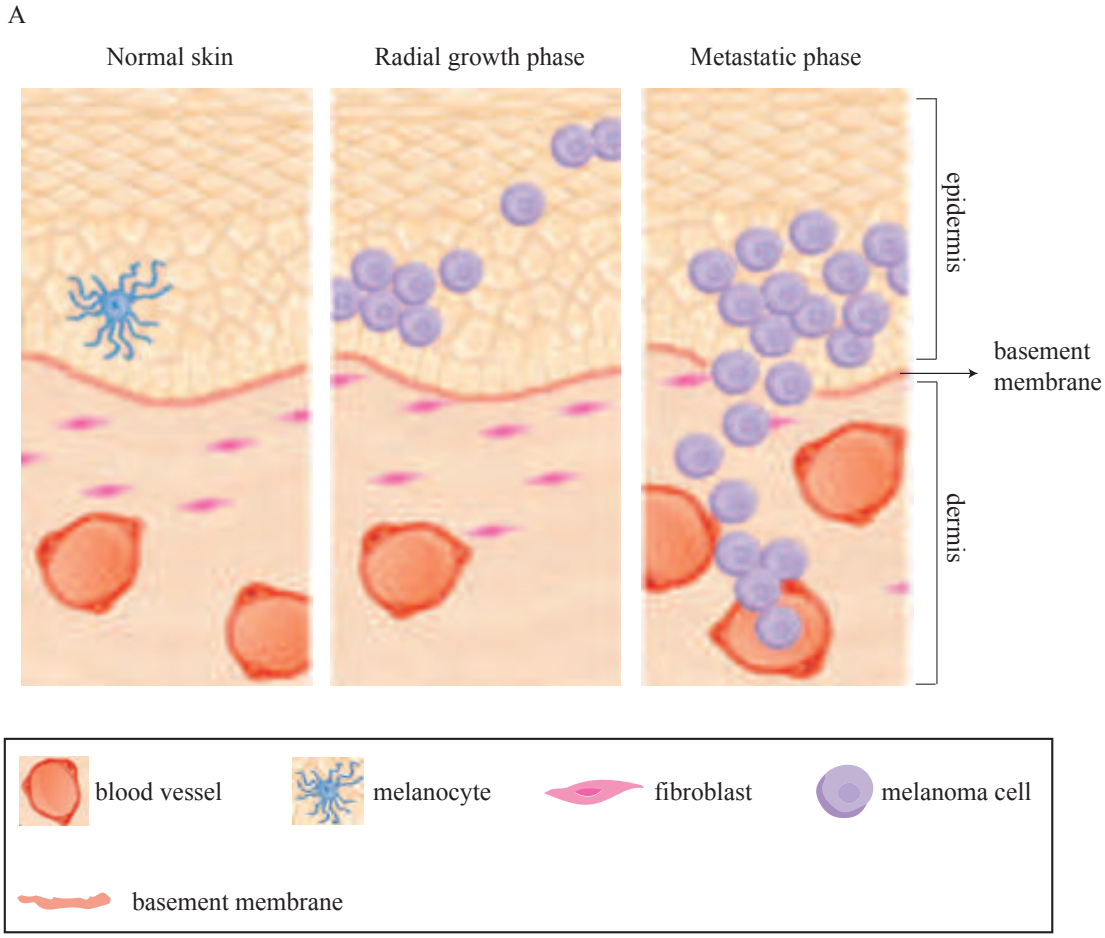

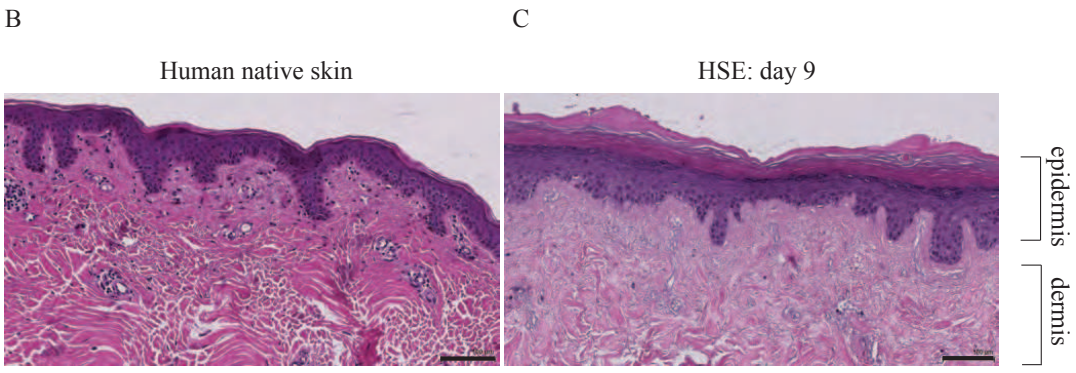

Figure 1: Three-dimensional representation of melanoma progression.

(A) Schematic representation of normal skin physiology illustrating the epidermal region with melanocytes and the dermal region with fibroblasts and blood vessels separated by a basement membrane. The RGP phase is associated with melanoma cells in the epidermal region only. The metastatic phase is associated with melanoma cells that move away from the primary site. The cells in the metastatic phase are able to cross the basement membrane, enter the dermis and move into the blood vessels. This illustration is adapted from Zaidi, Day & Merlino, (2008). (B) and (C) H&E staining of native human skin and HSE respectively, showing a well-defined epidermis and dermis. The scale bar corresponds to 100 μm.

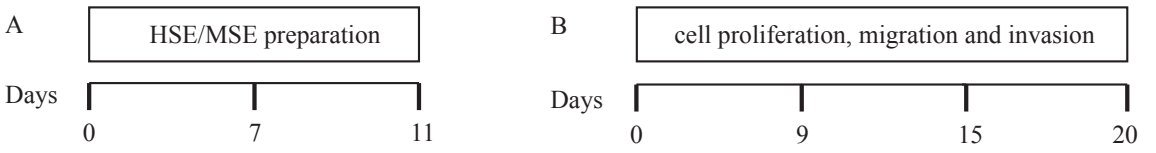

0-7 days: cell culture and DED preparation

7-11 days: adding cells to DED
and HSE/MSE submerged

day 0: HSE/MSE inspection time

day 9: HSE/MSE inspection time

day 15: HSE/MSE inspection time

day 20: HSE/MSE inspection time

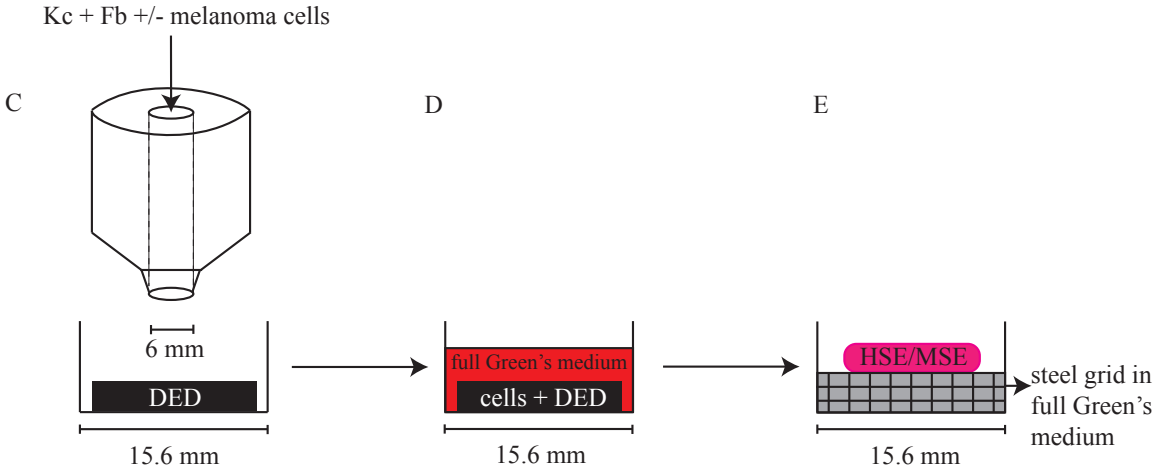

F

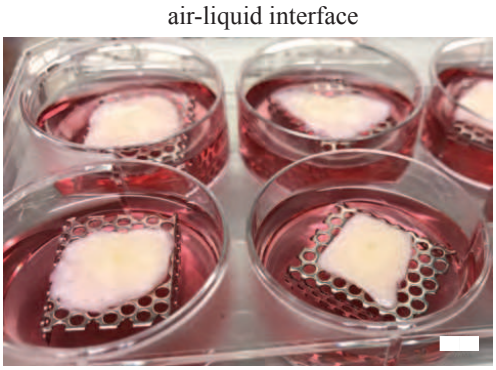

Figure 2: HSE and MSE preparation.

(A) Time frame for cell culture and DED preparation to construct HSE and MSE models. (B) Time intervals at which the HSE and MSE models are cultured and inspected. (C) Schematic of the circular barrier assay showing how cells are placed inside the barrier on a DED within a 24-well tissue culture plate. (D) DED with cells submerged in full Green's medium. (E)-(F) Schematic and image of the HSE and/or MSE models lifted to the air-liquid interface on a sterile stainless steel grid with full Green's medium placed in a 6-well plate. Scale in (F) bar corresponds to 6 mm.

PeerJ Preprints | https://doi.org/10.7287/peerj.preprints.2984v1 | CC BY 4.0 Open Access | rec: 19 May 2017, publ: 19 May 2017

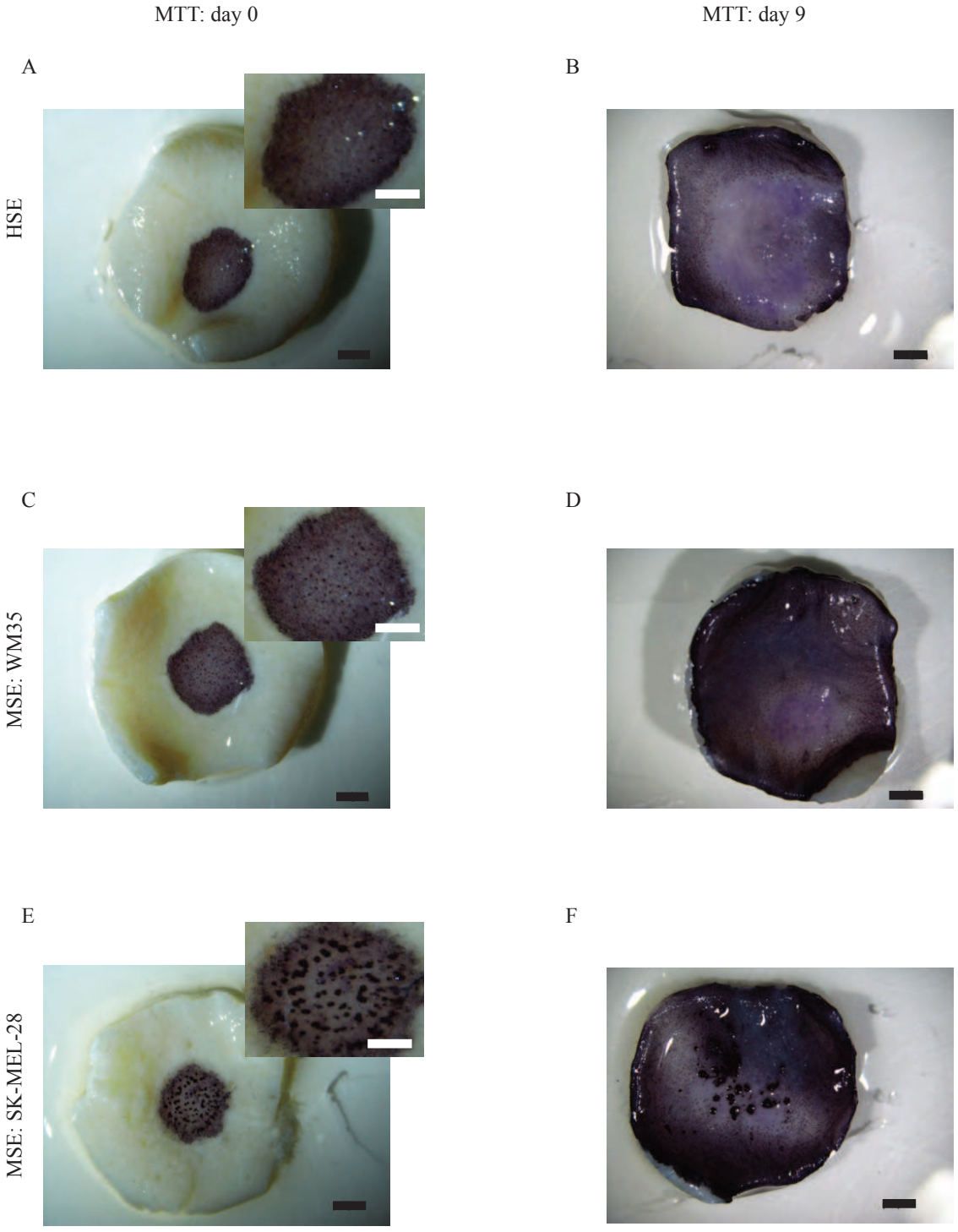

Figure 3: MTT assay.

Experimental images of the MTT assay shows viable cells (purple) on the HSE (A)-(B). The MSE with WM35 melanoma cells is shown in (C)-(D). The MSE with SK-MEL-28 melanoma cells is shown in (E)-(F). Results in the left column are at day 0, and results in the right column are at day 9. The magnified central region of the HSE and MSE with melanoma cell colonies is shown in the insets in (A), (C) and (E). Scale bars in the main image show 1 mm, whereas the scale bars in the insets show 3 mm.

Figure 4: Proliferation, migration and invasion of skin cells and WM35 melanoma cells.

(A)-(D) Proliferating cells (brown) highlighted by Ki-67 at day 0, 9, 15 and 20. (E)-(H) Migrating cells (brown) highlighted by vimentin. Dermal cells with elongated morphology are fibroblasts, and colonies of cells are migrating WM35 melanoma cells. (I)-(L) WM35 melanoma cells (brown) highlighted by S100 at day 0, 9, 15 and 20. Black arrows and inset images highlight positive staining. The scale bar in the main images shows 100 μm, and the width of the insets are approximately 75 μm.

Figure 5: Proliferation, migration and invasion of skin cells and SK-MEL-28 melanoma cells.

(A)-(D) Proliferating cells (brown) highlighted by Ki-67 at day 0, 9, 15 and 20. (E)-(H) Migrating cells (brown) highlighted by vimentin. Dermal cells with elongated morphology are fibroblasts, and colonies of cells are SK-MEL-28 melanoma cells. (I)-(L) SK-MEL-28 melanoma cells (brown) highlighted by S100 at day 0, 9, 15 and 20. Black arrows and inset images highlight positive staining. The scale bar in the main images shows 100 μm, and the width of the insets are approximately 75 μm.

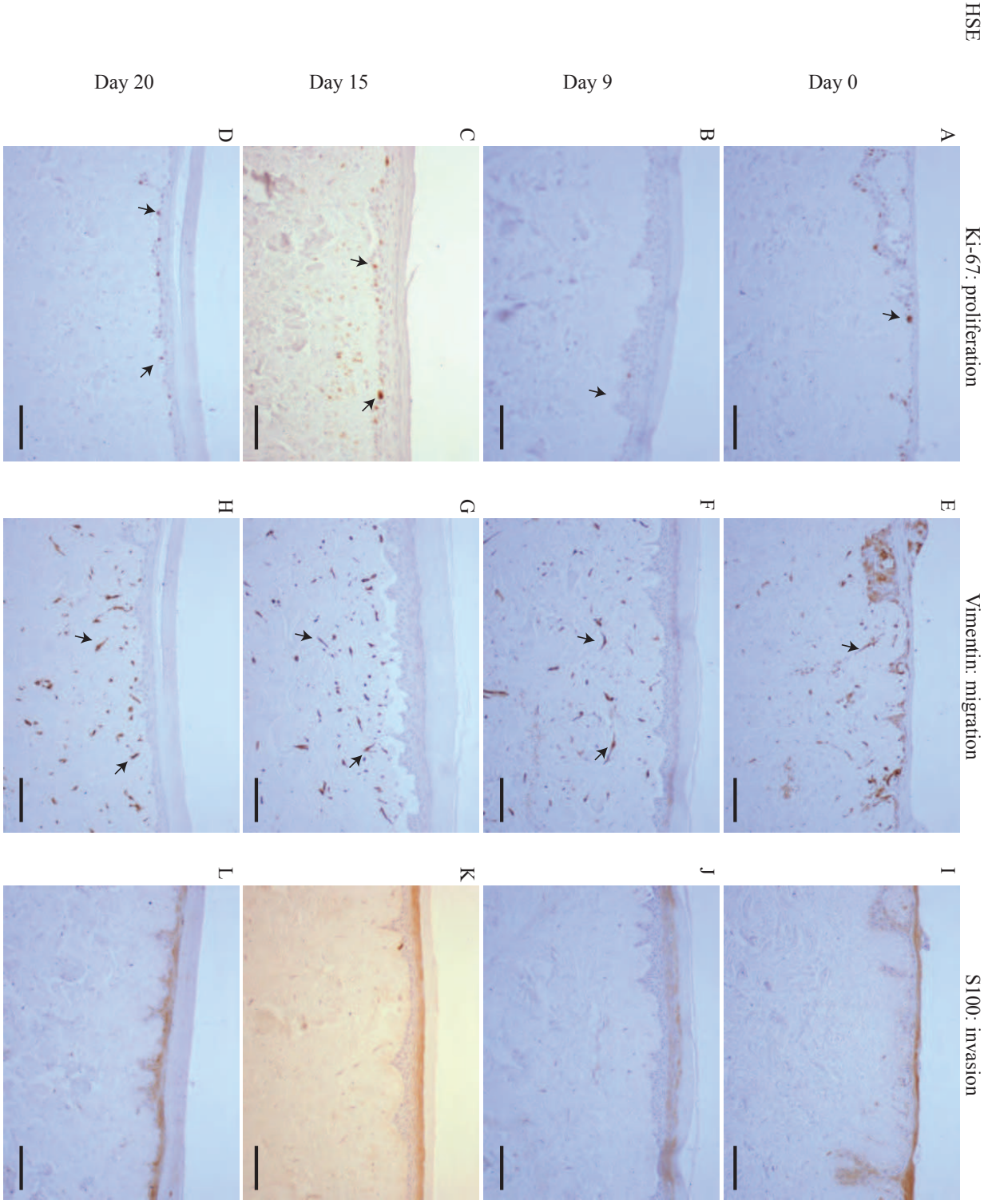

Figure 6: Proliferation, migration and invasion of skin cells.

(A)-(D) Proliferating cells (brown) highlighted by Ki-67 at day 0, 9, 15 and 20. (E)-(H) Migrating fibroblast cells (brown) highlighted by vimentin. (I)-(L) No specific melanoma staining is highlighted by S100 at day 0, 9, 15 and 20. Black arrows and inset images highlight positive staining. Scale bar corresponds to 100 μm.

PeerJ Preprints | https://doi.org/10.7287/peerj.preprints.2984v1 | CC BY 4.0 Open Access | rec: 19 May 2017, publ: 19 May 2017

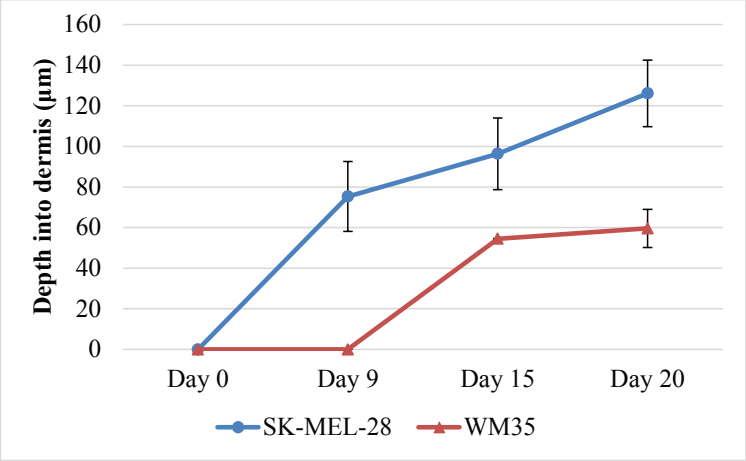

Figure 7: Quantification of melanoma cell invasion depth.

Depth of melanoma invasion for the WM35 (red) and SK-MEL-28 (blue) cell lines. Data points show the average depth of invasion. The error bars measure the variability, as given by the sample standard deviation. In each case the sample mean and sample standard deviation is calculated using measurements from at least nine (n=9) identically prepared experiments.

Previous Studies	Melanoma cell lines included			Comparison of MSE and HSE structure		Basement membrane marker	Proliferation marker	Migration marker	Melanoma marker	Measurements of invasion depth	Time course images
	RGP	VGP	Metastatic	Kc	Fb						
Bechetoille et al., 2000	no	no	yes	yes	no	yes	no	yes	yes	no	no
Eves et al., 2000	no	no	yes	yes	yes	yes	no	no	yes	no	no
Dekker et al., 2000	yes	yes	yes	yes	no	yes	no	no	yes	no	no
Mac Neil et al., 2000	no	no	yes	yes	yes	yes	no	no	yes	no	no
Eves et al., 2003a	no	no	yes	yes	yes	yes	no	no	yes	yes	no
Eves et al., 2003b	no	no	yes	yes	yes	yes	no	no	yes	yes	no
Dennhofer et al., 2003	no	no	yes	no	no	no	no	no	yes	no	no
Marck et al., 2005	no	no	yes	yes	yes	yes	no	no	yes	yes	no

Van-Kilsdonk et al., 2008	no	no	yes	yes	no	yes	no	no	yes	no	no
Yang, Sule-Suso & Sockalingum, 2008	no	no	yes	yes	yes	yes	no	no	yes	no	no
Van-Kilsdonk et al., 2010	no	no	yes	yes	no	yes	no	no	yes	no	no
Marques & Mac Neil, 2016	no	no	yes	yes	yes	yes	no	no	yes	yes	no
Current study	yes	yes	yes	yes	yes	yes	yes	yes	yes	yes	yes

Table1: Key features of previous 3D-DED melanoma skin model studies

Legend: Key properties of previous studies using 3D-DED to establish HSE and MSE models. Kc indicates primary keratinocyte cells, and Fb indicates primary fibroblast cells.

PeerJ Preprints | https://doi.org/10.7287/peerj.preprints.2984v1 | CC BY 4.0 Open Access | rec: 19 May 2017, publ: 19 May 2017

Primary Antibody				Antigen Retrieval Method		
Antibody	**Antibody type**	**Source**	**Dilution**	**Time and temperature**	**Buffer**	**Time and temperature**
Collagen IV (Col IV)	Mouse	DKSH, Australia	1:50	1 hour, 37 °C	Sodium Citrate (pH6.0)	20 minutes, 80 °C
Ki-67	Mouse	Sigma Aldrich, Australia	1:100	1 hour, 37 °C	EDTA (pH8.0)	30 minutes, 90 °C
Loricrin	Rabbit	Dako, Australia	1:100	1 hour, 37 °C	EDTA (pH8.0)	5 minutes, 97 °C
S100	Rabbit	Dako, Australia	1:3000	1 hour, 37 °C	Sodium Citrate (pH6.0)	5 minutes, 95 °C
Vimentin	Rabbit	Thermo Scientific, Australia	1:800	12 – 24 hours, 4 °C	Sodium Citrate (pH8.0)	20 minutes, 80 °C

Table 2: Primary antibody protocols

Legend: Details of the primary antibodies and the antigen retrieval method used to detect the basement membrane (Col IV); terminal epidermal differentiation (Loricrin); migration (Vimentin); proliferation (Ki-67); and invasion (S100).

PeerJ Preprints | https://doi.org/10.7287/peerj.preprints.2984v1 | CC BY 4.0 Open Access | rec: 19 May 2017, publ: 19 May 2017